ACS SENSORS

pubs.acs.org/acssensors Article

Recombinant Antibody Engineering Enables Reversible Binding for Continuous Protein Biosensing

Christian Fercher, Martina L. Jones, Stephen M. Mahler, and Simon R. Corrie*

Cite This: *ACS Sens.* 2021, 6, 764–776 Read Online

ACCESS | Metrics & More | Article Recommendations | Supporting Information

ABSTRACT: Engineering antibodies to improve target specificity, reduce detection limits, or introduce novel functionality is an important research area for biosensor development. While various affinity biosensors have been developed to generate an output signal upon varying analyte concentrations, reversible and continuous protein monitoring in complex biological samples remains challenging. Herein, we explore the concept of directed evolution to modulate dissociation kinetics of a high affinity anti-epidermal growth factor receptor (EGFR) single-chain variable antibody fragment (scFv) to enable continuous protein sensing in a label-free binding assay. A mutant scFv library was generated from the wild type (WT) fragment via targeted permutation of four residues in the antibody–antigen-binding interface. A single round of phage display biopanning complemented with high-throughput screening methods then permitted isolation of a specific binder with fast reaction kinetics. We were able to obtain ∼30 times faster dissociation rates when compared to the WT without appreciably affecting overall affinity and specificity by targeting a single paratope that is known to contribute to the binding interaction. Suitability of a resulting mutant fragment to sense varying antigen concentrations in continuous mode was demonstrated in a modified label-free binding assay, achieving low nanomolar detection limits (K_D = 8.39 nM). We also confirmed these results using an independent detection mechanism developed previously by our group, incorporating a polarity-dependent fluorescent dye into the scFv and reading out EGFR binding based on fluorescence wavelength shifts. In future, this generic approach could be employed to generate improved or novel binders for proteins of interest, ready for deployment in a broad range of assay platforms.

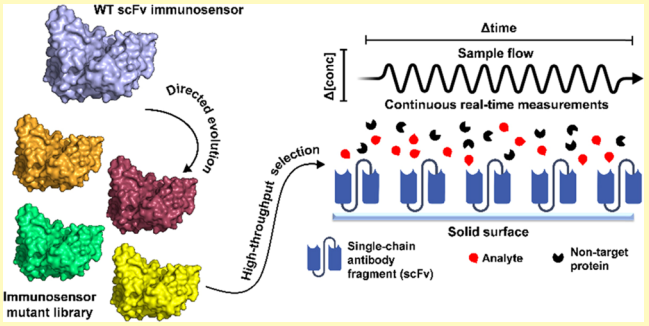

KEYWORDS: *antibody engineering, mutagenesis, continuous biosensing, label-free, unnatural amino acid*

The ability to monitor protein biomarker concentrations in body fluids in real-time would be invaluable for tracking patients at risk of rapid deterioration, including those requiring personalized drug monitoring,[1−5] or those at high risk of complications arising from critical conditions including sepsis, myocardial infarction, etc.[6,7] A range of new biosensors are emerging for detecting biomarkers continuously from both outside the body (e.g., via the skin, the eyes, and saliva)[8] and from inside the body (e.g., nanosensors and electrodes).[9−11] However, these techniques are currently limited to monitoring small molecules including drugs, neurotransmitters, and metabolites because technology for continuous protein biosensing is lacking. Plaxco and colleagues have recently shown the potential for continuous monitoring using affinity interactions—successfully demonstrating that DNA aptamers tethered to electrodes can reversibly bind therapeutic drugs for in vivo pharmacokinetics,[12] opening up new opportunities for personalized monitoring and closed-loop control.[2,13] While aptamers offer simple and inexpensive synthesis options, the use of reversible aptamers for continuous protein monitoring has not been reported until only recently.[14] The neutrophil gelatinase-associated lipocalin (NGAL)-binding sensor component described in this study was derived from a previously generated aptamer[15] by successively truncating the parent construct to achieve binding-induced conformational changes. Hence, it is difficult to assess if a similar strategy may be applied to other high affinity aptamers. In contrast, antibody and antibody fragment binders can be robustly designed and optimized using a wide variety of in vitro evolution approaches;[16−18] however, to our knowledge, such approaches have not been applied to the problem of generating reversible binders for continuous protein monitoring. Beyond the clinical environment, a reliable continuous sensing technology could further facilitate process optimization and control during the production of biologics in bioreactors or contribute to research analyzing nanomedicine translocation processes and compara-

Received: July 23, 2020
Accepted: January 11, 2021
Published: January 22, 2021

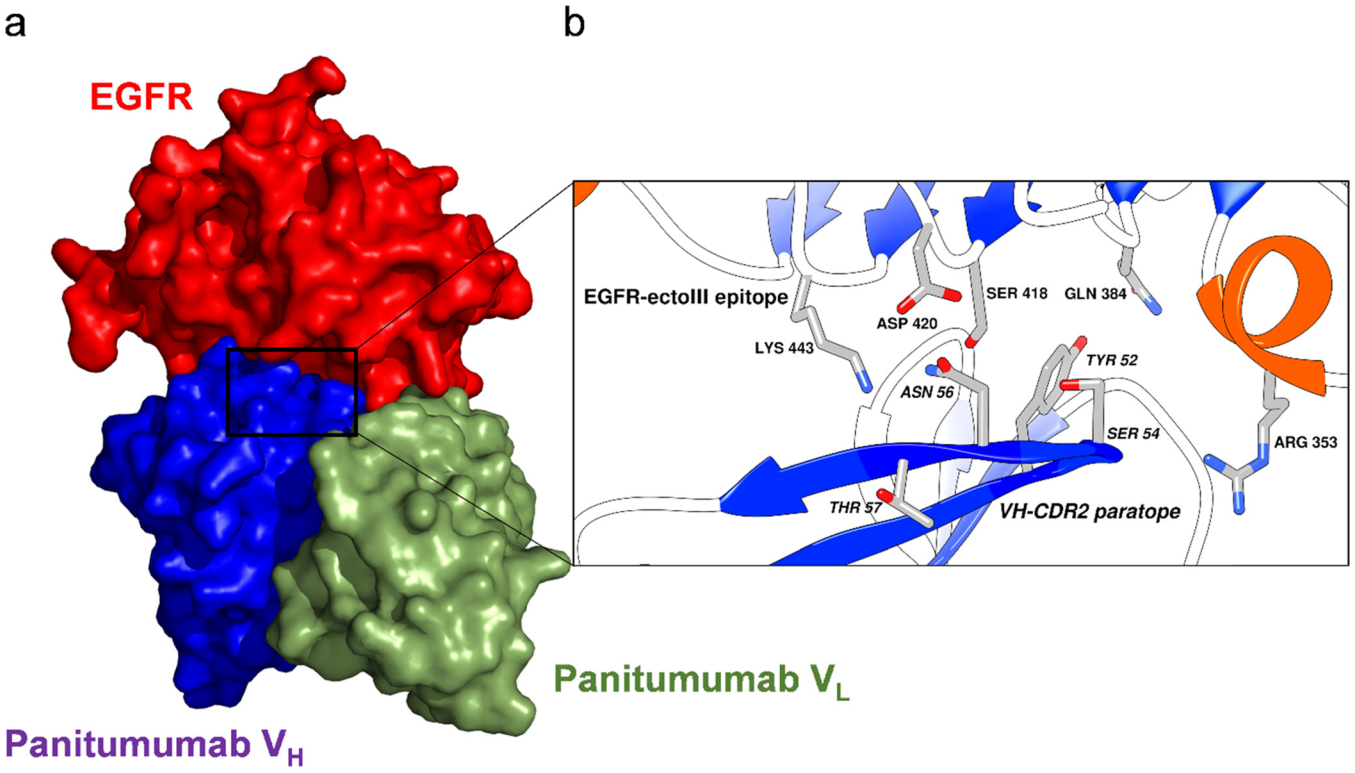

Figure 1. Crystallographic high-resolution structure (PDB 5SX4) of the panitumumab-EGFR complex. (a) VH and VL chains are depicted in blue and green, respectively, while the EGFR ectodomain 3 is colored in red. (b) Four residues in the VH-CDR2 paratope, Tyr-52, Ser-54, Asn-56, and Thr-57 (in italic) were selected to undergo one round of mutagenic permutation based on their vital contributions to epitope recognition and binding. Contact residues of the EGFR epitope are indicated.

tive expression of specific proteins under a wide variety of conditions.[19−21]

Examples of highly reversible antibodies are rare and so far exclusively based on the isolation of premature B cell clones following immunization of animals.[4,22,23] While isolated immunoglobulins displayed rapid dissociation, this approach resulted in relatively low affinity antibodies and relies on lengthy and expensive immunization/isolation procedures without the ability to engineer the final product. In contrast, recent developments in surface regeneration techniques allow the use of wild type (WT) antibodies for multiple analysis cycles over extended time periods (e.g., in SPR platforms), thereby reducing costs. However, this approach requires designated surface regeneration steps after each sample measurement and is thus not capable of real-time analysis.[24]

Additionally, utilization of a full monoclonal antibody (mAb) is further complicated by the bivalency of antibody molecules which can result in multiple interactions with corresponding antigen epitopes.[25] Consequently, apparent dissociation rates may be significantly slower than intrinsic dissociation which may impact on the ability of a specific candidate to be used as a sensing moiety in a continuous immunosensor.[4] One strategy to resolve this issue is to genetically combine the variable heavy (V_H) and light (V_L) chains, thereby creating a single-chain variable fragment (scFv) comprising only one antigen-binding site. Frequently, V_H and V_L are connected by a serine-glycine linker that provides spatial flexibility of the individual chains as well as low antigenicity when used as a therapeutic.[26] Reformatting an anti-myoglobin mAb with a remarkably fast dissociation rate into an scFv has been shown but resulted in a significant reduction in binding affinity and thus overall sensitivity.[23] Another strategy to circumvent limitations of bivalent antibodies is the use of variable heavy-chain-only antibodies (VHH) that are part of the immune repertoire of camelids. In fact, Saerens et al. (2004) demonstrated that high affinity binders with fast dissociation rates can be isolated from focused phage display libraries derived from an immunized dromedary.[27] However, to the best of our knowledge and despite the potential usefulness of these approaches, incorporation of an scFv or VHH in a continuous flow-based immunosensor has not yet been described. In previous work, we generated an scFv-based one-step optical immunosensor by genetic incorporation of a polarity indicator near the binding interface of an anti-epidermal growth factor receptor (EGFR) fragment, derived from the therapeutic mAb panitumumab (Vectibix).[28,29] Other groups have developed optical immunosensors using similar strategies relying primarily on changes in fluorescence intensity of a labeled antibody fragment in response to target binding.[30−32] Our approach enabled reagentless measurements of varying antigen concentrations in buffers spiked with 5% serum by following concentration-dependent emission wavelength shifts of the unnatural amino acid (UAA) Anap, site specifically incorporated into the binding site. However, due to the highly optimized binding affinity and markedly slow dissociation rate of the scFv, continuous analyte monitoring using surface immobilized fragments was futile.

In this study, we used a top-down approach to create an engineered antibody fragment capable of reversibly binding a protein analyte in dilute serum, retaining the apparent specificity of the WT sequence. Permutation of a single paratope within CDR2 of the variable heavy chain (V_H-CDR2) resulted in a library of fragments that was subjected to phage display

https://dx.doi.org/10.1021/acssensors.0c01510
ACS Sens. 2021, 6, 764−776

biopanning and affinity screening methods in order to isolate mutant clones with faster dissociation rates (k_d). This strategy resulted in the isolation of a mutant fragment with dissociation rates ~30 times faster than the WT. Furthermore, targeted engineering of a single paratope retained specificity of the mutant for the original antigen even in 10% serum conditions. Interestingly, the lower affinity of the mutant toward the antigen did not appear to affect nonspecific interactions with other serum analytes or homologous growth factor receptors. Reproducible continuous analyte monitoring was performed on a Biacore (SPR) system over the course of 11 h, and we confirmed this reversibility in a simple optical detection system using our previous approach of incorporating polarity-dependent dyes into the antigen-binding site. These results clearly demonstrate the feasibility of this pipeline to facilitate translation of an already existing high affinity (therapeutic) antibody into a reversible reagent for continuous sensing applications.

RESULTS

Structural Analysis and Library Construction. Engineering an antibody fragment for the purpose of increasing dissociation rates resembles strategies used in classic antibody affinity maturation campaigns. However, certain requirements when focusing on tuning kinetic rate constants (preservation of library diversity; selection toward fast dissociation rates over high affinity) require different approaches in library design and selection. In order to selectively weaken the stability of the antibody−antigen complex, we initially targeted a single complementary determining region (CDR) based on the published crystal structure of the panitumumab F(ab)2 fragment in complex with its antigen (PDB 5SX4—Figure 1a), the soluble extracellular domain of the EGFR.[33] Upon close inspection of the binding interface, we chose to permutate four residues (Tyr-52, Ser-54, Asn-56, and Thr-57 according to the Kabat numbering system)[34] in V_H-CDR2 as shown in Figure 1b. This decision was based on the following considerations: (1) V_H-CDR2 provides several important contact residues that seemed vital for the high affinity of this antibody. Hence, we were interested in exploring whether destabilizing this interaction network might increase dissociation rates without fundamentally affecting association rates. (2) Targeting a confined number of residues in a single CDR reduces the risk of emerging cross-reactivity, therefore preserving specificity of the scFv. (3) Tyr-53, which is a part of this paratope, was found to be the ideal position for the incorporation of an environmentally sensitive fluorophore that renders this fragment suitable for reagentless analyte sensing in solution.[29] As we aimed to combine both characteristics, i.e., reagentless and continuous analyte measurement capabilities, into a single sensor entity, Tyr-53 was excluded as a target residue for saturation mutagenesis. The resulting paratope comprising four residues was permutated using degenerate primers to generate a library of scFv mutants displaying a range of different off-rates. A combination of 21 possible substitutions at four positions generates a library with $\sim 1.16 \times 10^5$ distinct clones which lies well within the number of colonies routinely obtained when transforming a highly competent *E. coli* strain. Using a commercially available electrocompetent TG1 strain, we achieved a library size of $\sim 1.03 \times 10^8$ cfu as estimated from the transformation rate. Sequencing 20 randomly selected clones, we estimated the viability of the transformed library to be around 70−80%. Amber stop codon mutations at either of the four positions as well as frameshifts occurring within the targeted region constituted the primary reasons for nonviable clones. However, this might only be of concern if a larger number of residues is selected for permutation, thus reaching the limit of the bacterial transformation rate. Given the high level of redundancy we obtained when comparing the transformation rate and viability to the theoretical size of our library, we concluded that each possible clone is likely represented at least once within the final phage library used for biopanning.

Library Reduction by Phage Display Biopanning. To exclude nonfunctional variants from the initial library, we employed phage display biopanning as an initial screening method to enrich the mutational scFv library for clones that recognize the EGFR antigen. In contrast to classic antibody maturation campaigns where 3−4 panning rounds are routinely employed to reduce the starting phage pools to a minimal number of high affinity variants, we sought to exclude only those that do not bind the target antigen while preserving diversity within the phage pool. We applied a single round of panning, simultaneously testing three different elution conditions to separate bound phages from the immobilized antigen. By varying pH between 2.5, 4, and 5.3 at this point we sought to test the hypothesis whether milder elution conditions would reduce the number of isolated clones and favor the extraction of those with lower overall affinity but faster dissociation rates, as elution by pH variation is a common approach used in affinity maturation.[35] Screening the library and three elution pools in a polyclonal phage immunoassay (Figure 2a) did not reveal any differences in the relative binding strength of individual pools and only pH 2.5 and 5.3 pools were further analyzed in monoclonal phage immunoassays. Nevertheless, these results demonstrate that biopanning is a crucial step to remove a relatively large number of nonbinders from the library. While all three amplified elution pools did produce robust signals upon substrate conversion down to a phage dilution of 10^{-3}, only the undiluted (neat) phage library sample gave signals above the baseline when incubated with the antigen (Figure 2b).

Next, 90 individual clones were isolated from each of the three elution phage pools and binding was analyzed in a monoclonal phage ELISA (Supplementary Figure 1a−d) assessing recognition of the positive (EGFR-His) and negative (interleukin 22-His) antigens. As the number of clones to be evaluated in subsequent kinetic screening assays was limited and no significant difference in the ratio of positive to negative binders was found across pools, only binders isolated from pH 2.5 and 5.3 elution conditions were selected for a detailed analysis. In total, 53 phage clones with a monoclonal phage ELISA signal of at least 10% of the WT panitumumab-derived clone and a lack of signal for the negative antigen were purified and the titer of each sample was determined. An equal number of purified phages (5×10^8 cfu/well) was used for a comparative phage immunoassay to better assess relative affinities of these clones and to confirm results of the comparably crude monoclonal ELISA (Figure 2c). Purified phages were also used to transduce phagemids into *E. coli* HB2151. This strain does not produce scFv-pIII fusion proteins, thus eliminating sample heterogeneity in subsequent binding studies. With a focus on the isolation of clones with fast dissociation rates, we decided to assess all 53 clones in biolayer interferometry (BLI) experiments as they represented a wide spectrum of relative affinities when compared to the WT.

Screening Binding Kinetics of Library Clones with BLI. Following phage display biopanning, we subjected periplasmic extracts containing the WT and mutant scFvs to BLI binding

https://dx.doi.org/10.1021/acssensors.0c01510
ACS Sens. 2021, 6, 764−776

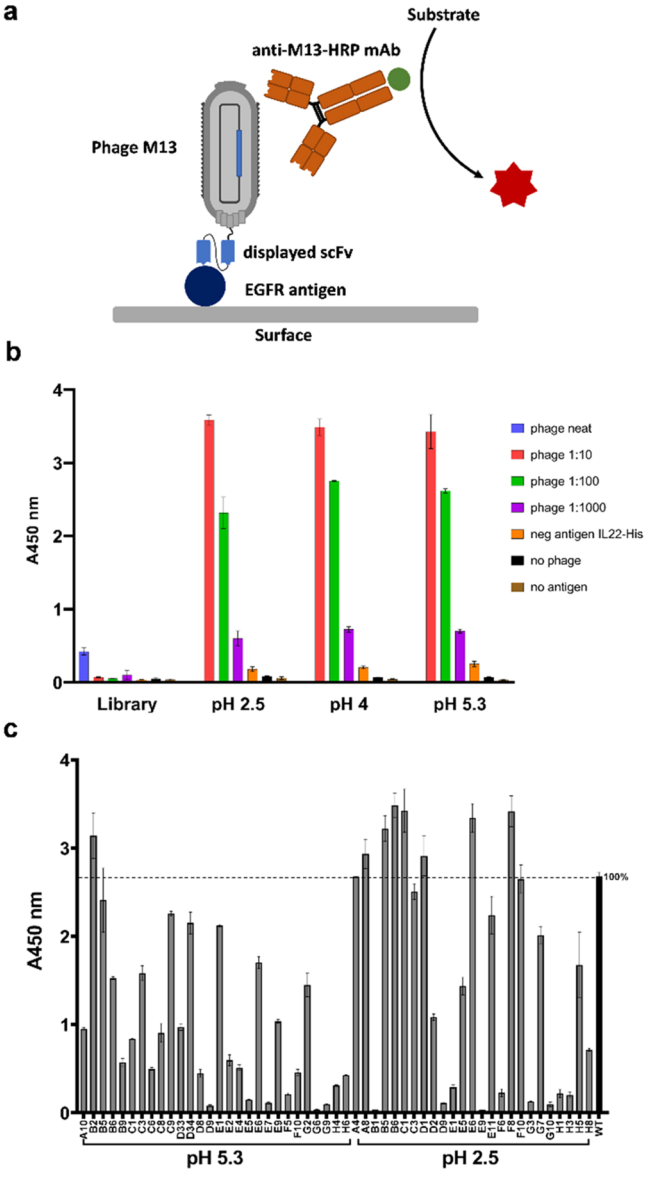

Figure 2. Enzyme immunoassay analysis of phage display biopanning experiments. (a) Schematic representation of a typical phage ELISA experiment. The target protein is coated onto the surface of an ELISA plate followed by blocking and incubation with scFv displaying phage particles. Phages are detected with an antiphage antibody conjugated to HRP. (b) Three different elution conditions were tested (pH 2.5, 4, and 5.3) and resulting pools were analyzed in a polyclonal phage ELISA. (c) In total, 53 positive phage clones of the pH 2.5 and 5.3 pools were isolated, purified, and assessed in a comparative phage ELISA using equal numbers of phage particles per sample. Data are presented as mean and ± SD of three independent replicates.

assays to further reduce the mutant pool based on the apparent affinities and off/on rates. This approach enabled fast assay optimization when immobilizing scFvs from crude bacterial extracts, as well as high-throughput measurements of purified analytes in a 96 well format under ideal buffer conditions. Bacterial protein expression and extraction yields were evaluated using western and dot blots. Proteins expressed in the HB2151 strain were detected as a single band following SDS-PAGE separation (Supplementary Figure 2a), and production levels of most mutants were largely consistent with those observed for the WT fragment (Supplementary Figure 2b). However, two clones of the pH 2.5 pool (B1 and D2) did not show any detectable signal and were excluded from BLI measurements. Following rounds of assay optimization, an analyte concentration of 31 nM was used to probe sensor-captured antibody fragments. A total number of 22 clones did not produce binding curves, could not be fitted using a 1:1 stoichiometry binding model or presented a R^2 value <0.9 and were excluded from further analysis. Apparent kinetic rate constants and equilibrium dissociation constants of the remaining 29 fragments and the WT are listed in Supplementary Table 3 and were mapped onto a rate plane plot with indicated isoaffinity diagonals (Figure 3a) for better comparison. Results demonstrated variations of k_a and k_d values over a full order of magnitude within the analyzed pool, resulting in dissociation constants in the low nanomolar range. Previous BLI measurements of the purified WT scFv produced an average affinity constant (K_D) value of 1.6×10^{-9} M which is in very good agreement with the numbers obtained in previous studies (1.58×10^{-9} M).[29] In total, six clones (sensorgrams shown in Supplementary Figure 3) with apparent dissociation rates close to and above 10^{-2} s^{-1} were selected for in-depth analysis by surface plasmon resonance (SPR).

Detailed Analysis of Binding Kinetics with SPR. In order to streamline kinetic and subsequent continuous measurements, we used immobilized antipolyhistidine antibodies to capture scFvs purified from mammalian supernatants (Supplementary Figure 4a) on a CM5 Biacore chip. This strategy enabled the use of the same chip to determine binding and dissociation rates of all clones in a single experiment, regenerating the sensor surface between measurements. Initially, single cycle kinetics were performed to estimate the K_D of each construct to adjust analyte concentrations in multicycle experiments (Figure 3b). Despite the marked differences of mutant k_a and k_d values when compared to the WT in BLI experiments, five variants (D33, E11, F10, G3, and H5) displayed similar kinetics in the range of the original scFv (Supplementary Figure 4b). However, mutations in clone E5 caused a significant increase of the dissociation rate with little impact on association kinetics resulting in a K_D in the low nanomolar range (Figure 3c). According to these results, antigen dissociation is about ~30 times faster for E5 than for the WT fragment accounting for an antibody−antigen half-life of approximately 4.4 min (t_{90} = 14.6 min). This is in stark contrast to the 126.5 min half-life of the WT complex (t_{90} = 420.3 min) and suggested suitability of this clone for continuous measurements of varying analyte concentration without the need of intermediate regeneration cycles.

Specificity Analysis of the WT and Mutant Fragment. Despite initial efforts to minimize effects on antigen specificity by mutating a limited number of residues in a single CDR loop, concerns were raised whether specificity of the E5 mutant toward the original EGFR antigen would be compromised. Consequently, ELISA binding studies were performed, supplying either the EGFR or the soluble extracellular domain of two homologous growth factor receptors in 10% human serum (Supplementary Figure 5a). Both purified WT and E5 scFvs produced signals significantly above the baseline when probed with the EGFR but bound neither the vascular endothelial growth factor receptor 2 (VEGFR2) nor the fibroblast growth factor receptor (FGFR). These results suggested that E5 retained specificity for the original antigen with reliable and precise detection even in 10% serum conditions. The difference in signal between WT and mutant fragments is consistent with results obtained from SPR measurements, reflecting the lower

https://dx.doi.org/10.1021/acssensors.0c01510
ACS Sens. 2021, 6, 764−776

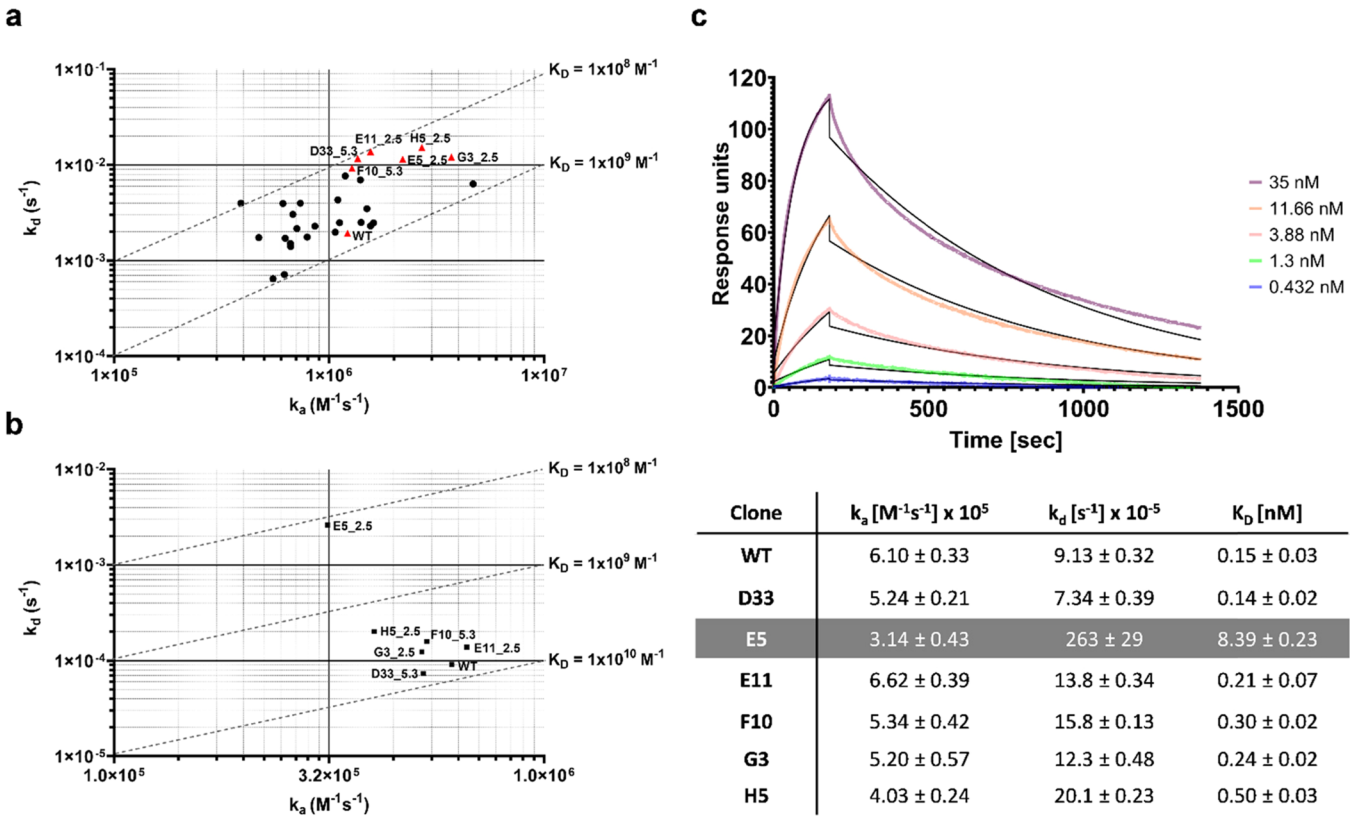

Clone	k_a [M^{-1}s^{-1}] x 10^5	k_d [s^{-1}] x 10^{-5}	K_D [nM]
WT	6.10 ± 0.33	9.13 ± 0.32	0.15 ± 0.03
D33	5.24 ± 0.21	7.34 ± 0.39	0.14 ± 0.02
E5	3.14 ± 0.43	263 ± 29	8.39 ± 0.23
E11	6.62 ± 0.39	13.8 ± 0.34	0.21 ± 0.07
F10	5.34 ± 0.42	15.8 ± 0.13	0.30 ± 0.02
G3	5.20 ± 0.57	12.3 ± 0.48	0.24 ± 0.02
H5	4.03 ± 0.24	20.1 ± 0.23	0.50 ± 0.03

Figure 3. Mutant scFv E5 displays a ∼30-fold faster dissociation rate than the WT fragment. (a) Rate plane plot with isoaffinity diagonals of 29 scFv fragments captured from periplasmic extractions that produced evaluable association and dissociation curves (R^2 of the fit >0.9) in BLI binding assays. The WT and six mutants with rapid apparent dissociation rates close to and above 10^{-2} s^{-1} are shown and indicated (Δ). Suffixes indicate affiliation to either the pH 2.5 or 5.3 elution pools, respectively. Data are presented as mean of two independent experiments. Detailed binding kinetics of all clones are presented in Supplementary Table 3. (b) Rate plane plot indicating binding and dissociation kinetics of the WT and the six mutant fragments purified from mammalian supernatants as measured by SPR. Clone E5 displayed a dramatically improved dissociation rate while the other mutant scFvs were relatively similar to the WT. (c) SPR sensorgram of E5. Purified antibody fragments were captured onto one channel of the sensor chip surface via immobilized antipolyhistidine antibodies and probed with five EGFR concentrations. Sensorgrams were corrected against blank runs and the signal of the reference channel was subtracted before curve fitting using a 1:1 surface binding model. Association (k_a) and dissociation (k_d) constants were calculated and used to obtain the affinity constant K_D. Sensorgrams of the WT and the other mutants are presented in Supplementary Figure 4. Data are given as mean ± SD of three independent measurements.

overall affinity of the E5 clone. To further analyze binding characteristics of the E5 fragment in these conditions, SPR binding studies were repeated supplying EGFR diluted in assay buffer supplemented with 10% human serum (Supplementary Figure 5b,c). Global fitting of the resulting sensorgrams indicated that association and dissociation rates and therefore overall affinity of E5 is consistent regardless of the complexity of the sample matrix, further confirming the ability of the mutant to precisely sense the EGFR with high specificity and affinity under more complex conditions.

Continuous and Reversible Analyte Monitoring via SPR. To investigate the potential for continuous analysis in a reversible manner, we immobilized the E5 and WT fragments via their polyhistidine tags noncovalently to CM5 sensor chips and introduced the EGFR antigen in sweeps of increasing and then decreasing concentrations. Based on a relatively high dissociation rate constant, the E5 fragment but not the WT was able to accurately reproduce alternating antigen concentrations when fragments were captured on the chip surface via His-tags (Supplementary Figure 6). Following covalent immobilization of the scFvs onto the chip surface, we were able to reproducibly monitor varying protein concentrations over the course of roughly 11 h, allowing 10 min of association followed by 10 min dissociation per sample (Figure 4a). Based on an initial ligand immobilization of 5500 RU, we could reliably detect as little as 0.5 nM EGFR in modified assay buffer. We found that a covalent immobilization approach was required in order to remove the effect of baseline drift and decline of ligand density due to dissociation of the anti-His mAb−scFv complex on the chip surface. In addition, a modified assay buffer containing 0.2% SDS and 0.05% Tween 20 was used to minimize nonspecific binding and analyte aggregation close to the chip surface. Preliminary experiments in the absence of SDS frequently caused pronounced nonideal binding at higher analyte concentrations during the association phase. A dose response curve was constructed from data points at the end of each association phase and showed high consistency of individual concentrations within three full injection cycles (Figure 4b). The coefficient of variance (% CV) of the normalized data set was in the range of 2.3−16.1% demonstrating good reproducibility. Furthermore, plotting the individual sensorgrams of a single measurement cycle within the same timeframe of 1000 s demonstrated that sensor response rates were suitable to stabilize the signal during association and dissociation in the measured concentration range (Figure 4c). It is important to note that nonideal binding patterns at higher antigen

https://dx.doi.org/10.1021/acssensors.0c01510
ACS Sens. 2021, 6, 764−776

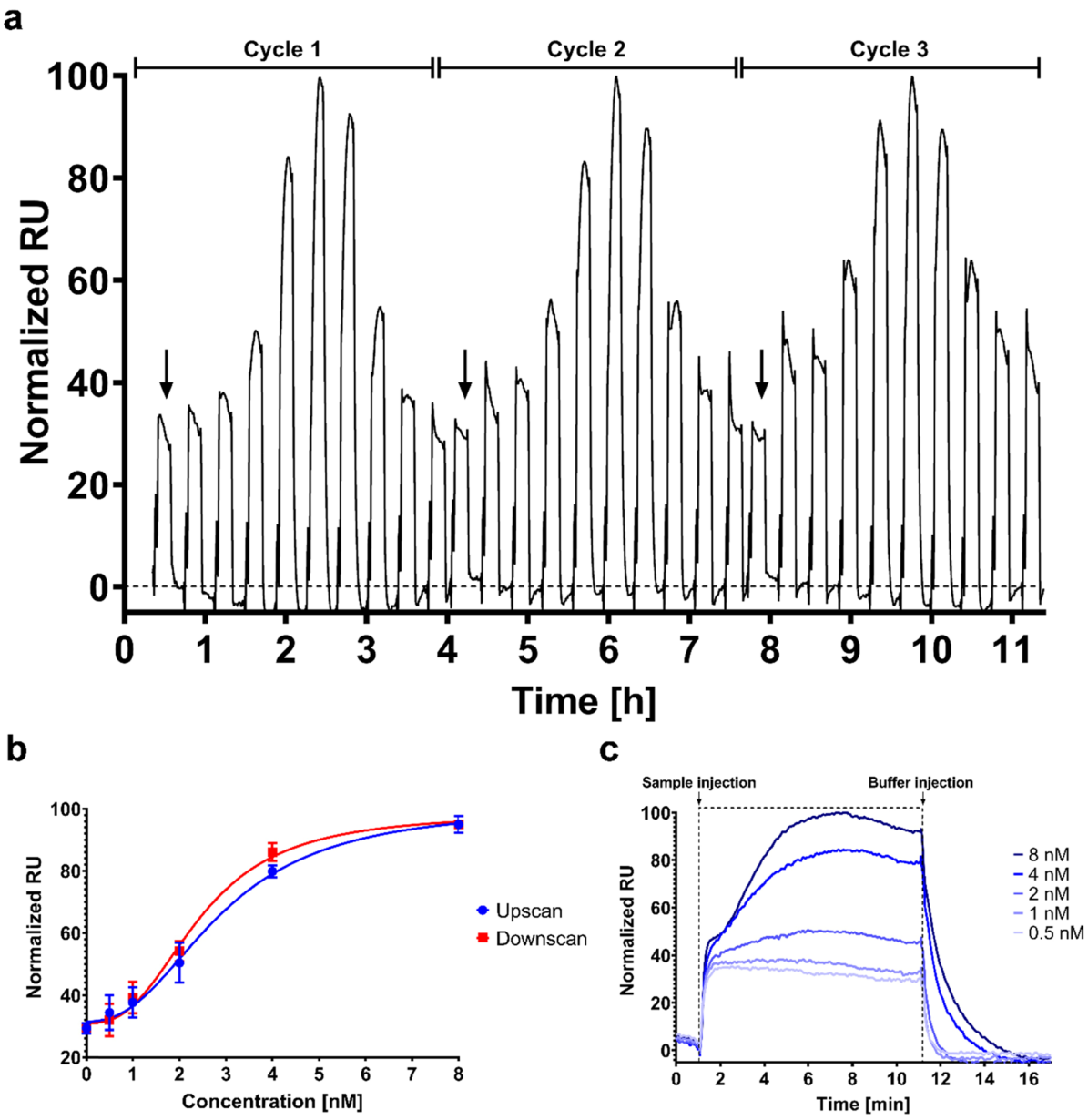

Figure 4. Continuous analyte monitoring applying varying concentrations of the EGFR in a modified SPR assay. (a) Direct immobilization of E5 to the chip surface enabled stable and continuous measurement of three cycles of varying analyte concentrations in the tested range (0, 0.5, 1, 2, 4, and 8 nM) over the course of 11 h. Sensorgrams were normalized between the first data point before injection representing the baseline and the highest datapoint of the data set. Arrows indicate buffer injections (0 nM analyte) for which the assay buffer was supplemented with protein sample buffer to control for bulk shifts caused by small differences in the refractive index. Cycle durations of 10 min association followed by 10 min dissociation were found to be optimal for baseline stabilization. (b) Signal of each dose was averaged and used to construct a dose−response curve for association (upscan) and dissociation (downscan), showing hysteresis. The coefficient of variance(CV) for all measurements was between 2.3 and 16.1%. Data are plotted as mean and ± SD of three (0 and 8 nM) and six (0.5, 1, 2, and 4 nM) measurement points, respectively. Data points were fitted with a nonlinear regression model in Graphpad Prism 8. (c) Upscan preinjection baselines, association, and dissociation phases of the first measurement cycle normalized to a timeframe of 17 min. Sample and buffer injection time points are indicated to demonstrate the response of the sensor. Generally, 10 min for association and about 6 min for dissociation are necessary to sufficiently stabilize the signal in the measured concentration range.

concentrations emerge. This effect is most likely caused by the high ligand density on the sensor chip surface and was, in part, mitigated by employing the optimized assay buffer and a 10 min association phase.

Reversible Analyte Monitoring with an Alternate Detection Approach. In order to independently confirm our results on the reversible binding of the E5 mutant, we employed our previous strategy of incorporating a polarity-dependent fluorophore into the fragment to monitor analyte binding based on the fluorescence wavelength shift. Previously, we demonstrated that incorporation of the UAA Anap at a specific position in the WT scFv generates a titratable emission wavelength blue shift upon incubation of the fragment with the analyte. In the current study, this was achieved by transiently cotransfecting two mammalian expression plasmids into Expi293 (HEK) cells, one harboring the antibody fragment including a TAG stop codon mutation in lieu of Tyr-53 and the other coding for an amber suppressor tRNA, as well as the synthetase AnapRS, respectively.[36] Kinetic parameters ($k_a = 1.56 \times 10^5$; $k_d = 1.97 \times 10^{-3}$) and K_D (1.27×10^{-8}) were established in single-cycle SPR

https://dx.doi.org/10.1021/acssensors.0c01510
ACS Sens. 2021, 6, 764−776

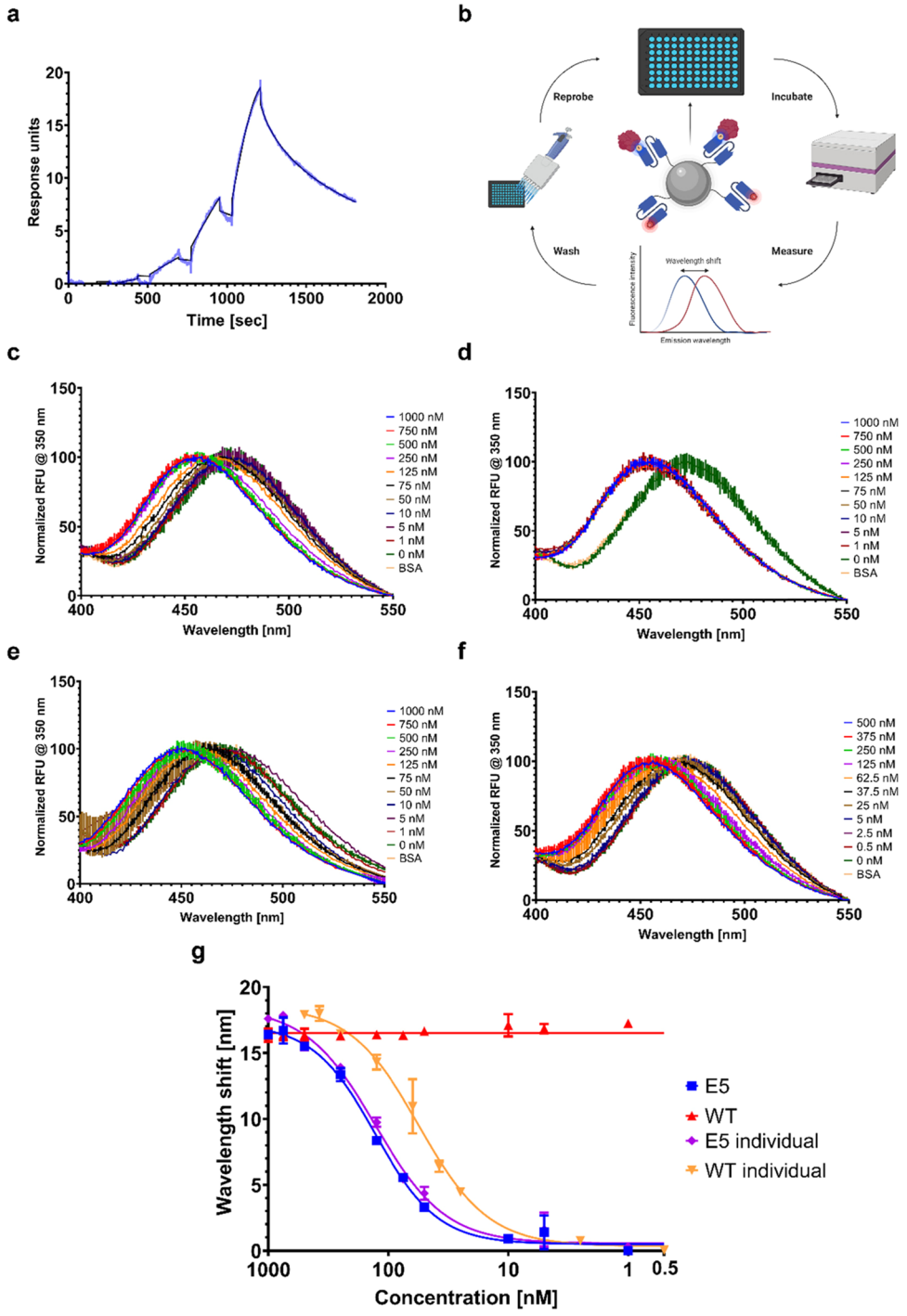

Figure 5. Reversible protein binding measurements via optical emission wavelength shifts. (a) Single-cycle kinetic SPR analysis of the E5-Anap scFv. Kinetic parameters ($k_a = 1.56 \times 10^5$; $k_d = 1.97 \times 10^{-3}$) and K_D (1.27×10^{-8}) are in good agreement with the values obtained for the unlabeled fragment. (b) Antibody fragments were immobilized on Ni-NTA beads and incubated with the highest antigen concentration. Following excitation at 350 nm, fluorescence spectra were recorded between 400 and 550 nm. Beads were washed 1× in PBS supplemented with 0.05% Tween 20 for 5 min and reprobed with successively lower analyte concentrations. While E5 (c) reacts to decreasing EGFR concentrations due to fast dissociation kinetics, the WT (d) does not. In parallel, individual E5 (e) and WT (f) samples were incubated with the antigen to demonstrate almost complete reversibility for the E5 fragment and that blue-shifting is generally detectable for the WT within the measured concentration range. (g) Observed wavelength shifts were used to construct concentration-dependent binding curves for each experiment reflecting E5 responsiveness. Spectra and binding curves are presented as mean and ± SD of three independent experiments which were fitted with the Laurentzian nonlinear regression model in Graphpad Prism 8 to obtain the amplitudes of the individual data sets.

experiments (Figure 5a) and were found to be in good agreement with values obtained for the unlabeled fragment. To demonstrate reversibility, the scFv was immobilized on Ni-NTA resin via its C-terminal hexahistidine tag and initially probed with a high antigen concentration followed by 5 min wash steps and incubation with successively lower analyte concentrations. Emission spectra were recorded at each concentration step following excitation of the fluorophore at

https://dx.doi.org/10.1021/acssensors.0c01510
ACS Sens. 2021, 6, 764−776

350 nm. Baseline emission spectra were recorded in the absence of the EGFR and 1 μM bovine serum albumin (BSA) was used as the negative control (Figure 5b). The resulting spectra and time-dependent binding curves were compared to those obtained for the WT fragment. In this set up, the E5 fragment displayed a reduction of the observable emission blue shift when interrogated with decreasing antigen concentrations at each step (Figure 5c,g). This is due to the fast dissociation rate of the antibody−antigen complex which causes almost complete removal of the bound antigen during the intermediate washing steps. Conversely, no wavelength shift was detectable when the WT fragment was used in the same experimental setup as dissociation of the complex is remarkably slow (Figure 5d,g). In order to demonstrate blue-shifting of the E5 (Figure 5e) and WT (Figure 5f) fragments within this concentration range, individual scFv samples were incubated with varying antigen concentration. A clear concentration-dependent blue shift was observed under these conditions comparable to the results obtained previously.[29] Interestingly, higher antigen concentrations were required in a bead-based assay to achieve similar wavelength shifts as observed in solution,[29] likely due to mass transport limitations on the solid-phase which was not optimized as is the case for SPR approaches. However, this is the first report to our knowledge that demonstrates the fluorescence detection mechanism performed on the solid phase. The combination of results from SPR and fluorescence measurements independently confirm that the E5 clone serves as a reversible protein binder, the first to our knowledge which has been generated using a directed evolution approach.

DISCUSSION

A fundamental requirement for a continuous biosensor is a reagent which can reversibly bind to the analyte of interest, in this case an scFv with a fast dissociation rate. Such a binder could be isolated using de novo biopanning of a naïve scFv library; however, it is challenging to optimize a biopanning strategy which both selects for high overall affinity and fast dissociation rates. As an alternative approach, we have started with a high affinity scFv and engineered the fragment utilizing directed evolution to select for mutants with fast dissociation rates. This shows that a high affinity antibody can be engineered to bind reversibly to protein analytes at low concentrations, facilitating continuous monitoring over multiple hours in vitro. To demonstrate the proof of concept, we selected a panitumumab-derived antibody fragment and its corresponding antigen, the extracellular domain of the EGFR, as a model system. This immune complex has been studied in great detail and the availability of a high-resolution crystal structure proved beneficial, especially in the initial stage of the project.[28,33] Naturally, the success of protein engineering can be considerably enhanced by selectively targeting entire domains or individual residues based on functional and/or structural data. Antibodies provide a unique advantage as residues required for antigen binding can be identified by sequence analysis as they are almost exclusively located in the CDR loops. Hence, the availability of structural information can be helpful when targeting specific residues while the absence of such does not necessarily preclude a successful outcome. Lou and Marks outlined several principal guidelines regarding affinity maturation of antibodies that, despite having an antibody−antigen structure at hand, were used as a guideline during the selection of target residues.[37] The accuracy of their approach may be further enhanced by utilizing homology-based structural models which are relatively reliable due to the limited conformational diversity of framework regions and five of the six CDR antigen-binding loops.[38] In fact, light chain CDRs L1-L3 and heavy chain CDRs H1 and H2 can be subdivided into a small set of discrete conformational classes known as canonical structures.[39] Numerous studies led to the identification of structure-determining residues at certain positions, which allows for the prediction of the canonical class from sequence with high accuracy. However, CDR H3 has not been classified into canonical forms as a considerable range of different structures has been observed. Nonetheless, several ab initio modeling approaches, some ameliorated with knowledge-based conformational constraints, have been suggested to improve the spatial orientation of the modeled H3 regions.[40] However, in the absence of a high-resolution complex structure, several CDRs may have to be targeted to isolate a promising mutant for continuous sensing applications.

We mutated four residues in V_H-CDR2 to tune dissociation kinetics of mutant clones. Using degenerate primers to permutate the respective codons, all possible combinations of amino acids should, in theory, be represented in the resulting mutant library. However, influenced by the subsequent selection process, a limited amount of sequence variability was observed in the final pool of sequenced mutants. In general, Tyr-52 and Ser-54 appear to be particularly important for the recognition of the EGFR epitope as they showed conservation scores of 80 and 66%, respectively (Supplementary Table 4). This is expected as both residues are part of an extended hydrogen bond network that significantly contributes to the stability of the intermolecular binding interface. Positions 56 and 59 are far more dynamic as these loci experienced substitutions to all other amino acid except Cys, Lys, and Gln. In clone E5, three out of four residues are changed (S54T, N56M, and T57V) with a conservative mutation present at position 54. The annotated WT scFv sequence and V_H-CDR2 variations of the characterized mutants can be found in Supplementary Table 4. The binding interface of the mutant scFv-EGFR complex was further characterized by in silico mutational analysis using the FoldX force field and program suite.[41] Multiple conformations of the introduced residues, as well as alternative conformations of surrounding residues are considered, and the energetically most favorable structure is presented (Supplementary Figure 7). Close inspection of the E5-EGFR interaction surface revealed that Thr-54 is still able to engage in a hydrogen bond with the Arg-353 in the EGFR epitope. Met-56 and Val-57 do not provide any inter- and intramolecular contacts due to their hydrophobic sidechains and might even exert destabilizing effects on the complex in solution. In fact, Met-56 appears to be the primary reason for the increased dissociation rate of clone E5 as its long hydrophobic side chain is directly positioned between the binding interface of the antibody and antigen. Surprisingly, substitutions to Leu in clones D33 and G3 and Ala in clone H5, albeit hydrophobic in nature, did not have a similar effect. This may be explained by a potential methionine-aromatic (S/π) interaction between the Met-56 sulfur atom and the aromatic sidechains of neighboring Tyr-52, Tyr-53, or both (S/π-bridge). These types of interactions are commonly found in structurally characterized proteins and could result in decreased flexibility of the V_H-CDR2 binding loop, simultaneously preventing either of the two tyrosine residues from engaging in H-bonds with the antigen.[42] These results underline the importance of individual residues for the stability of an antibody−antigen complex and demonstrate that their careful selection was crucial to efficiently modify binding kinetics. They also illustrate the significance of

https://dx.doi.org/10.1021/acssensors.0c01510
ACS Sens. 2021, 6, 764−776

only targeting a single paratope for saturation mutagenesis as further interference with the antibody/antigen-binding interface might have had detrimental effects on complex stability.

Accordingly, reduction of sequence diversity in the mutant library was shown to be crucial for consecutive steps to eliminate a considerable number of apparently nonfunctional binders (Figure 2b). In addition to scFv variants comprising nonsense mutations or frameshifts, permutation of residues in an important binding loop of an antibody will inevitably lead to the emergence of clones that fail to recognize the original antigen. In contrast to common phage display-based affinity maturation campaigns that routinely employ up to five rounds of biopanning,[43] a single round sufficed to deplete the elution pools of nonfunctional candidates. This approach further preserves sequence diversity of the library for a second selection step entirely based on binding kinetics. In this study, we made use of the high-throughput screening capabilities of an Octet RED96 instrument that employs biolayer interferometry to determine kinetic rate constants during molecular complex formation. In principle, BLI assays can be set up in two orientations, employing either the antibody or antigen as the ligand while probing the sensor tip with the opposite partner as the analyte. While global benchmark studies demonstrated that consistent results can be obtained regardless of the ligand−analyte orientation employing sufficiently optimized assay parameters and purified interaction partners,[44] utilization of bacterial extracts does not implicitly satisfy these conditions. We based our decision to capture the scFv on the sensor surface, subsequently using purified EGFR-Fc as the analyte on the following considerations. While k_d is independent of the analyte concentration and can be obtained in either of the above-mentioned experimental designs, determination of k_a and thus K_D relies on prior knowledge of analyte concentrations. As we attempted to isolate binders with fast dissociation rates paralleled by high overall affinities, determination of association kinetics as part of this screening step is desirable. Furthermore, capturing polyhistidine-tagged scFvs from periplasmic extracts via a sensor-immobilized anti-His antibody (HIS1K sensor) reduced interference by *E. coli* proteins during the actual binding assay and enabled the use of a similar capture approach in SPR assays using anti-His antibodies immobilized on a CM5 sensor chip. Nevertheless, only one out of six candidates identified by BLI displayed significantly faster dissociation rates than the WT when reanalyzed in more detailed SPR binding studies. This may be attributed to the change from a bacterial to a mammalian expression system and by further employing purified proteins rather than bacterial extracts for SPR and continuous analyte monitoring experiments. In contrast to bacteria, the mammalian protein folding machinery is far more sophisticated and better equipped to deal with the production of functional antibody fragments.[45−47] Conceivably, a significant amount of misfolded and thus non- or only partially functional antibody fragments may have been extracted from the bacterial periplasm in these cases. This notion is corroborated by the observation that dissociation constants and underlying kinetic parameters using purified components are generally reproducible on both instruments in our lab and beyond.[48] Interestingly, no significant differences in association and dissociation kinetics could be found between clones isolated from pH 2.5 and 5.3 elution pools. In fact, the narrow distribution of obtained overall dissociation constants presented in Supplementary Table 3 suggests that exploration of this parameter may be omitted in future engineering projects. Our results are comparable to success rates seen in related studies in which reversible antibodies were isolated from premature B cells of immunized animals. In these cases, one suitable candidate each was found screening a total number of 20 and 22 hybridoma clones, respectively.[4,22] In general, the screening of hundreds and even thousands of clones to find a single suitable candidate is not unheard of in classic antibody discovery and affinity maturation campaigns;[43] a task that, if required, can be accomplished with the herein described approach.

According to SPR analysis, complex half-life of the isolated E5 mutant was ∼30 times lower (t_{50} = 4.4 min; t_{90} = 14.6 min) than that of the WT fragment (t_{50} = 126.5 min; t_{90} = 420.3 min). Previous attempts to construct an scFv-based continuous biosensor derived from a premature anti-myoglobin antibody yielded similar results in terms of observed half-life (t_{50} = 1.8 min; t_{90} = 6.2 min) but provided significantly lower target affinity and thus limits of detection.[23] In contrast, premature full-length antibodies specifically developed for the detection of myoglobin and cardiac troponin I (cTnI) both displayed longer complex half-lives of 30 min (t_{90} = 99.4 min) and 7.1 min (t_{90} = 23.7 min), respectively, highlighting the suitability of our top-down engineering approach to develop a reversible binding fragment. Beyond antibodies, DNA aptamers have emerged as a promising and inexpensive biosensing strategy in the field of precision medicine,[49] with Plaxco's group recently reporting the first reversible aptamer system for protein detection.[14] Coupled to an electrochemical transducer while exploiting conformational changes in the sensing DNA strand, several experimental platforms with high sensitivity and specificity for varying target molecules have been described in the past decade.[50−53] Notably, selection of target specific aptamers by SELEX (systematic evolution of ligands by exponential enrichment) is more time-consuming and costly than employing equivalent display technologies for antibody engineering projects as described here.[54] Site-specific engineering of promising candidates is further complicated by the inability to identify binding sites from primary sequence analysis alone, representing a major obstacle for the development of a continuous biosensor. Critically, signaling of electrode-bound DNA probes relies on a binding specific change in the physics of the aptamer and has been shown to be relatively insensitive to the mere absorption of the target or contaminants to the probe head, thus enabling quantitative measurements in complex matrices such as whole blood, serum, or milk.[50,52] This is in contrast to techniques that tether recognition of a biomolecule to a surface to measure the change in the refractive index (e.g., SPR), wavelength interferometry (e.g., BLI), mass (e.g., quartz crystal microbalance), or charge (e.g., field-effect transistor-based sensors). While SPR, BLI, and related approaches are popular in specific fields, we sought to expand the utility of the reversible binding fragment by incorporating the polarity-dependent Anap dye into the sequence to enable protein binding based on fluorescence wavelength shifts. It is important to emphasize that the experiment employed in this study was not designed to meet the demands of a translatable assay but was focused on demonstrating that fast dissociation kinetics enable reversible protein sensing. In comparison, other groups have successfully employed fluorophores to monitor protein binding via changes in fluorescence intensity;[30−32] however, these examples do not facilitate reversible or continuous sensing, and intensity changes are more prone to environmental and instrumental noise. However, it is encouraging that a range of optically active antibody fragments have now been generated, and we expect

https://dx.doi.org/10.1021/acssensors.0c01510
ACS Sens. 2021, 6, 764−776

that these will be incorporated into more assays and devices in future, to cut down on the number of steps required to complete protein detection and biosensing experiments.

In conclusion, we have demonstrated that scFv fragments can be engineered to display reversible binding kinetics appropriate for continuous protein biosensing. Previously, only premature WT antibodies had shown this behavior, and it was not known if this property could be engineered. High-throughput characterization of the binding kinetics identified a lead compound, E5, for which we demonstrated continuous EGFR sensing in an SPR system. We also demonstrated the proof of concept reversible EGFR binding using the same fragment labeled with a polarity-dependent fluorescent dye. Currently, the use of Anap restricts concentration measurements to a moderately complex sample matrix due to its optimal excitation wavelength being in the UV range of the electromagnetic spectrum, causing substantial background fluorescence on nontarget proteins and cells. However, work is underway to employ dyes which are less affected by optical interference from serum components. In future, we expect that this process can be used to generate a range of reversible binders for many different protein analytes, to be incorporated into a range of bioassay platforms.

METHODS

Details for all primers, plasmids, and bacterial strains along with a detailed descriptions of protein expression, purification, and characterization are provided in Supporting Information.

Mutational scFv Library Preparation for Phage Display Biopanning. Four codons in V_H-CDR2 of a panitumumab-derived scFv (heavy chain residues 1−119 of GI 1073549642; light chain residues 1−107 of GI 1073549641) were randomized using V_HCDR2 random fwd and rev primers (Supplementary Table 2) which had target codons substituted for NNS combinations of nucleotides. N stands for any of the four possible nucleotides while S represents either G or C bases. This approach prevents ochre (TAA) and opal (TGA) stop codons from being introduced in the sequence which would decrease the viability of the resulting library. Parental DNA was removed by DpnI digestion and the DNA was end phosphorylated using poly nucleotide kinase (NEB). The linear plasmid was purified and circularized using T4 ligase (NEB) in an overnight reaction at 16 °C. Ligation reactions were desalted and transformed into electrocompetent *E. coli* TG1 cells (Lucigen) according to manufacturer's instructions. A small aliquot was used to determine transformation efficiency and estimate library size. The rest of the transformation was streaked on two large (Ø 150 mm) 2YT plates containing 100 μg/mL ampicillin and 2% glucose (2YT-AmpGlu) to suppress transcription of the phage pIII protein. Following overnight incubation at 37 °C, transformed bacteria were collected by washing plates with a total volume of 4 mL 2YT-AmpGlu supplemented with 20% glycerol. The optical density at 600 nm (OD_{600}) of the library was determined before storing aliquots at −80 °C.

To generate the phage library, 50 mL 2YT-AmpGlu was inoculated with the TG1 phage stock to an OD_{600} of 0.05. Bacteria were grown to an OD_{600} of 0.7 at 37 °C, 200 rpm and phage production was induced by adding a 10× excess of helper phage M13K07 (NEB). The suspension was incubated stationary at 37 °C for 30 min followed by another 30 min at 37 °C, 200 rpm. Infected bacteria were collected by centrifugation and resuspended in 100 mL 2YT supplemented with 100 μg/mL ampicillin and 30 μg/mL kanamycin (2YT-AmpKan). Phages were amplified overnight at 30 °C, 200 rpm and separated from bacterial cells by centrifugation on the following day. Phage particles were purified from the culture supernatant by two rounds of PEG/NaCl precipitation as described elsewhere.[55] The phage titer was determined by infecting an exponentially growing *E. coli* XL1-blue culture with serial dilutions of purified library phage. Infected bacteria were plated on 2YT-AmpGlu plates and colonies were counted following overnight incubation at 37 °C.

Phage Display Biopanning. One round of biopanning was performed against EGFR-His as described previously.[55] In brief, immunotubes (Nunc Maxisorp, Thermo Fischer Scientific) were coated overnight with 2 × 10 μg interleukin 22-His (negative antigen) and 10 μg EGFR-His (positive antigen) followed by a series of washes with PBS. The tubes were blocked with 1% casein in PBS (CPBS) for 1 h at room temperature (RT). Simultaneously, 4×10^{11} phages containing the mutational anti-EGFR scFv library were blocked in 1% CPBS. After 1 h, the blocked phages were sequentially added to the two negative antigen tubes to deplete the pool from potential binders against the His-tag followed by addition to the positive antigen tube to isolate binders specific for the extracellular domain of the EGFR. Incubation of each tube was 1 h at RT. Before elution of bound phages, tubes were washed three times with PBS + 0.1% Tween 20 and 3× with PBS. Finally, bound phages were eluted from the positive antigen tube by incubation with either 1 mL 100 mM glycine pH 2.5, 4, or 5.3 for 8 min at RT. The phage eluate was immediately neutralized using 500 μL of 1 M Tris, pH 7.4 and either directly used for phage amplification or stored at −80 °C after the addition of glycerol to a final concentration of 20% (v/v).

Phage pool amplification and titer determination was carried out in *E. coli* XL1 as described for phage library generation.

Biolayer Interferometry Binding Studies. *E. coli* periplasmic extracts containing the WT or mutant antibody fragments were obtained as described above and directly used for BLI binding studies. Experiments were conducted on an Octet Red96 platform (ForteBio). Extracted scFvs were captured on His1K biosensors (ForteBio) followed by a 600 s baseline stabilization step. EGFR-Fc prepared in assay buffer (PBS, 0.05% Tween 20, 0.05% casein, pH 7.4) at a concentration of 31 nM was used to probe the kinetics of the individual clones using an association time of 300 s and a dissociation time of 400 s. Sensorgrams were processed and fitted using Data Analysis 9.0 software (ForteBio).

Surface Plasmon Resonance Binding Studies. All multicycle kinetic (MCK) and continuous analyte monitoring studies were performed on a Biacore T200 instrument (Biacore Life Sciences, GE Healthcare). For MCK experiments, a CM5 sensor chip was used together with the His capture kit (GE Healthcare) according to manufacturer's instructions. Commercially available HBS-P^+ buffer (10 mM HEPES, 150 mM NaCl, 0.05% Surfactant P20; GE Healthcare) was used as running buffer and to dilute the ligand and analyte. Purified scFvs were captured on the surface of flow channel 2 via immobilized anti-His antibodies. The same amount of anti-His antibody was immobilized on flow channel 1 which served as a reference channel due to the absence of the captured scFv ligand throughout the experiments. The sensorgram of association and dissociation of EGFR-Fc consisted of a series of five analyte concentrations ranging from 0.1 to 10 times the estimated affinity constant (K_D) as determined in preliminary experiments. Data were corrected by subtraction of blank runs and curves were fitted using a 1:1 surface binding model in BIAevaluation software (Biacore Life Sciences, GE Healthcare). Global fitting was used to determine the association (k_a) and dissociation (k_d) rate constants and an overall K_D was calculated. The sensor surface was regenerated between runs using 60 s injections of 10 mM glycine, pH 1.5. MCK experiments in serum were conducted in the same manner but analytes were diluted in HBS-P^+ buffer supplemented with 10% human serum (Sigma-Aldrich).

Continuous analyte monitoring experiments were performed using covalent immobilization of the scFv onto the sensor surface. The scFv E5 was diluted to 50 μg/mL in 10 mM acetate, pH 4.5 and covalently attached via amine coupling onto EDC/NHS-activated sensor chip surfaces. Ethanolamine hydrochloride, pH 8.5 was subsequently injected to quench the remaining reactive groups. The same procedure was used to prepare the reference flow channel (#1), immobilizing similar amounts of an unrelated scFv, raised against the prostate-specific membrane antigen PSMA, onto the chip surface. Varying analyte concentrations were injected over both flow channels #1 and #2 to enable direct detection of a reference subtracted signal. To control for bulk shifts caused by the injection of sample matrices with a slightly different refractive index than the assay buffer used during dissociation

https://dx.doi.org/10.1021/acssensors.0c01510
ACS Sens. 2021, 6, 764−776

steps, the 0 nM analyte sample was diluted with the same amount of protein sample buffer as was used to prepare the actual protein containing injection samples.

Semicontinuous Binding Assays Based on Anap Fluorescence Spectra Measurements. Binding studies were performed as previously described[29] with the following deviations. Labeled scFv (1.5 μg) was immobilized on HisPur Ni-NTA resin (Thermo Fisher) by incubating a 50 nM protein sample with 10 μL resin. To prevent nonspecific interactions of the fluorophore-labeled antigen-binding interface with the resin surface, a PBS-based assay buffer had to be supplemented with 0.05% Tween 20 (PBST). The resin was transferred to a well of a black 96-well plate (Costar) that had been blocked with 5% milk powder for 1 h at RT. Fluorescence spectra were measured on a Tecan plate reader between 400−550 nm upon excitation of the fluorophore at 350 nm. After measurements, the resin was transferred to an empty Illustra Quant G50 micro column from which the original Sephadex resin had been removed. This setup allowed for repeated washing and incubation steps of the same scFv sample with minimal resin loss throughout the experiment. Next, the resin was incubated with BSA for 5 min at RT and spectra were measured after transferring the resin back to a different well of the 96-well plate. The resin was washed 1× in PBST for 5 min before addition of the highest antigen concentration. Spectra measurements, washing, and antigen incubation steps were repeated with decreasing antigen concentrations. For the individual WT control samples, 12 separate samples were immobilized in triplicates and incubated with varying analyte concentrations, assay buffer, or BSA, respectively.

■ ASSOCIATED CONTENT

Supporting Information

The Supporting Information is available free of charge at https://pubs.acs.org/doi/10.1021/acssensors.0c01510.

Bacterial strains and plasmids (Table S1); oligonucleotides (Table S2); apparent rate constants of scFv clones as measured with BLI (Table S3); WT scFv sequence, conservation of the VH-CDR2 paratope and VH-CDR2 sequences (Table S4); monoclonal phage ELISA results (Figure S1); western and dot blot analysis of bacterial scFv expression (Figure S2); BLI sensorgrams of selected clones with fast dissociation kinetics (Figure S3); SDS-PAGE and western blot analysis of purified scFv clones and SPR binding analysis of selected clones (Figure S4); specificity analysis of WT and E5 clones by ELISA and SPR (Figure S5); continuous analyte monitoring with noncovalently captured scFvs in SPR (Figure S6); and structural analysis of the WT and mutants paratopes (Figure S7) (PDF)

■ AUTHOR INFORMATION

Corresponding Author

Simon R. Corrie − *Department of Chemical Engineering, ARC Centre of Excellence in Convergent Bio-Nano Science and Technology, Monash University, Clayton, Victoria 3800, Australia;* orcid.org/0000-0001-8029-1896; Email: simon.corrie@monash.edu

Authors

Christian Fercher − *Australian Institute for Bioengineering and Nanotechnology, ARC Training Centre for Biopharmaceutical Innovation, The University of Queensland, St. Lucia, Queensland 4072, Australia; Australian Institute for Bioengineering and Nanotechnology, ARC Centre of Excellence in Convergent Bio-Nano Science and Technology, The University of Queensland, St. Lucia, Queensland 4072, Australia*

Martina L. Jones − *Australian Institute for Bioengineering and Nanotechnology, ARC Training Centre for Biopharmaceutical Innovation, The University of Queensland, St. Lucia, Queensland 4072, Australia*

Stephen M. Mahler − *Australian Institute for Bioengineering and Nanotechnology, ARC Training Centre for Biopharmaceutical Innovation, The University of Queensland, St. Lucia, Queensland 4072, Australia*

Complete contact information is available at: https://pubs.acs.org/10.1021/acssensors.0c01510

Author Contributions

S.R.C., C.F., M.L.J., and S.M.M. conceived and initiated the project. S.R.C. supervised the study. C.F. designed experiments, with input from M.L.J. C.F. conducted the experiments, analyzed the data, and prepared the figures. C.F. wrote the manuscript. All authors edited and S.R.C. approved the manuscript.

Notes

The authors declare no competing financial interest.

■ ACKNOWLEDGMENTS

This project utilized the scientific and technical assistance of the National Biologics Facility (NBF) at the University of Queensland. NBF is supported by Therapeutic Innovation Australia (TIA). TIA is supported by the Australian Government through the National Collaborative Research Infrastructure Strategy (NCRIS) program. The authors also acknowledge funding from the Australian Research Council through the ARC Centre of Excellence in BioNano Science (S.R.C).

■ ABBREVIATIONS

BLI, biolayer interferometry; CDR, complementarity determining region; scFv, single-chain variable fragment; EGFR, epidermal growth factor receptor; FGFR, fibroblast growth factor receptor; PSMA, prostate specific membrane antigen; RU, response unit; SPR, surface plasmon resonance; VEGFR, vascular endothelial growth factor receptor

■ REFERENCES

(1) Arroyo-Curras, N.; Dauphin-Ducharme, P.; Ortega, G.; Ploense, K. L.; Kippin, T. E.; Plaxco, K. W. Subsecond-Resolved Molecular Measurements in the Living Body Using Chronoamperometrically Interrogated Aptamer-Based Sensors. *ACS Sens* **2018**, *3*, 360−366.

(2) Dauphin-Ducharme, P.; Yang, K.; Arroyo-Curras, N.; Ploense, K. L.; Zhang, Y.; Gerson, J.; Kurnik, M.; Kippin, T. E.; Stojanovic, M. N.; Plaxco, K. W. Electrochemical Aptamer-Based Sensors for Improved Therapeutic Drug Monitoring and High-Precision, Feedback-Controlled Drug Delivery. *ACS Sens* **2019**, *4*, 2832−2837.

(3) Jing, W.; Wang, Y.; Yang, Y.; Wang, Y.; Ma, G.; Wang, S.; Tao, N. Time-Resolved Digital Immunoassay for Rapid and Sensitive Quantitation of Procalcitonin with Plasmonic Imaging. *ACS Nano* **2019**, *13*, 8609−8617.

(4) Kim, D. H.; Paek, S. H.; Lim, G. S.; Jeon, J. W.; Paek, S. H. Performance characteristics of monoclonal antibodies as recyclable binders to cardiac troponin I. *Anal. Biochem.* **2012**, *431*, 11−18.

(5) Kim, D.-H.; Seo, S.-M.; Cho, H.-M.; Hong, S.-J.; Lim, D.-S.; Paek, S.-H. Continuous immunosensing of myoglobin in human serum as potential companion diagnostics technique. *Biosens. Bioelectron.* **2014**, *62*, 234−241.

(6) Aydin, S.; Ugur, K.; Aydin, S.; Sahin, İ.; Yardim, M. Biomarkers in acute myocardial infarction: current perspectives. *Vasc Health Risk Manag* **2019**, *15*, 1−10.

(7) Opal, S. M.; Wittebole, X. Biomarkers of Infection and Sepsis. *Crit. Care Clin.* **2020**, *36*, 11−22.
(8) Yang, Y.; Gao, W. Wearable and flexible electronics for continuous molecular monitoring. *Chem. Soc. Rev.* **2019**, *48*, 1465−1491.
(9) Harvey, J. D.; Williams, R. M.; Tully, K. M.; Baker, H. A.; Shamay, Y.; Heller, D. A. An in Vivo Nanosensor Measures Compartmental Doxorubicin Exposure. *Nano Lett.* **2019**, *19*, 4343−4354.
(10) Le, L. V.; Chendke, G. S.; Gamsey, S.; Wisniewski, N.; Desai, T. A. Near-Infrared Optical Nanosensors for Continuous Detection of Glucose. *J. Diabetes Sci. Technol.* **2020**, *14*, 204−211.
(11) Wang, D.; Xiao, X.; Xu, S.; Liu, Y.; Li, Y. Electrochemical aptamer-based nanosensor fabricated on single Au nanowire electrodes for adenosine triphosphate assay. *Biosens. Bioelectron.* **2018**, *99*, 431−437.
(12) Arroyo-Currás, N.; Somerson, J.; Vieira, P. A.; Ploense, K. L.; Kippin, T. E.; Plaxco, K. W. Real-time measurement of small molecules directly in awake, ambulatory animals. *Proc. Natl. Acad. Sci. U. S. A.* **2017**, *114*, 645−650.
(13) Arroyo-Currás, N.; Ortega, G.; Copp, D. A.; Ploense, K. L.; Plaxco, Z. A.; Kippin, T. E.; Hespanha, J. P.; Plaxco, K. W. High-Precision Control of Plasma Drug Levels Using Feedback-Controlled Dosing. *ACS Pharmacol. Transl. Sci.* **2018**, *1*, 110−118.
(14) Parolo, C.; Idili, A.; Ortega, G.; Csordas, A.; Hsu, A.; Arroyo-Currás, N.; Yang, Q.; Ferguson, B. S.; Wang, J.; Plaxco, K. W. Real-Time Monitoring of a Protein Biomarker. *ACS Sens* **2020**, *5*, 1877−1881.
(15) Wang, J.; Yu, J.; Yang, Q.; McDermott, J.; Scott, A.; Vukovich, M.; Lagrois, R.; Gong, Q.; Greenleaf, W.; Eisenstein, M.; et al. Multiparameter Particle Display (MPPD): A Quantitative Screening Method for the Discovery of Highly Specific Aptamers. *Angew. Chem., Int. Ed. Engl.* **2017**, *56*, 744−747.
(16) Franklin, E.; Cunningham, O.; Fennell, B. in *Antibody Engineering: Methods and Protocols* (eds Nevoltris, D.; Chames, P.) 457−477 (Springer New York, 2018). DOI: 10.1007/978-1-4939-8648-4_23.
(17) Könning, D.; Kolmar, H. Beyond antibody engineering: directed evolution of alternative binding scaffolds and enzymes using yeast surface display. *Microb. Cell Fact* **2018**, *17*, 32.
(18) Lai, J. R.; Chen, G.; Sidhu, S. S. in *Struct Bio Immun* (eds Putterman, C.; Cowburn, D.; Almo, S.) 81−100 (Academic Press, 2018). DOI: 10.1016/B978-0-12-803369-2.00003-6.
(19) Jia, B.; McNeil, L. K.; Dupont, C. D.; Tsioris, K.; Barry, R. M.; Scully, I. L.; Ogunniyi, A. O.; Gonzalez, C.; Pride, M. W.; Gierahn, T. M.; et al. Longitudinal multiparameter single-cell analysis of macaques immunized with pneumococcal protein-conjugated or unconjugated polysaccharide vaccines reveals distinct antigen specific memory B cell repertoires. *PLoS One* **2017**, *12*, No. e018373.
(20) Selby, L. I.; Aurelio, L.; Yuen, D.; Graham, B.; Johnston, A. P. R. Quantifying Cellular Internalization with a Fluorescent Click Sensor. *ACS Sens* **2018**, *3*, 1182−1189.
(21) Zitzmann, J.; Weidner, T.; Eichner, G.; Salzig, D.; Czermak, P. Dielectric Spectroscopy and Optical Density Measurement for the Online Monitoring and Control of Recombinant Protein Production in Stably Transformed Drosophila melanogaster S2 Cells. *Sensors* **2018**, *18*, 900.
(22) Kim, D. H.; Seo, S. M.; Paek, S. H.; Lim, G. S.; Paek, S. H. Premature antibodies with rapid reaction kinetics and their characterization for diagnostic applications. *Anal. Biochem.* **2012**, *420*, 54−60.
(23) Song, H.-N.; Jang, J.-H.; Kim, Y.-W.; Kim, D.-H.; Park, S.-G.; Lee, M. K.; Paek, S.-H.; Woo, E.-J. Refolded scFv antibody fragment against myoglobin shows rapid reaction kinetics. *Int. J. Mol. Sci.* **2014**, *15*, 23658−23671.
(24) Kim, D. H.; Cho, I. H.; Park, J. N.; Paek, S. H.; Cho, H. M.; Paek, S. H. Semi-continuous, real-time monitoring of protein biomarker using a recyclable surface plasmon resonance sensor. *Biosens. Bioelectron.* **2017**, *88*, 232−239.
(25) Nieba, L.; Krebber, A.; Pluckthun, A. Competition BIAcore for measuring true affinities: large differences from values determined from binding kinetics. *Anal. Biochem.* **1996**, *234*, 155−165.
(26) Fercher, C.; Keshvari, S.; McGuckin, M. A.; Barnard, R. T. Evolution of the magic bullet: Single chain antibody fragments for the targeted delivery of immunomodulatory proteins. *Exp. Biol. Med. (Maywood)* **2018**, *243*, 166−183.
(27) Saerens, D.; Kinne, J.; Bosmans, E.; Wernery, U.; Muyldermans, S.; Conrath, K. Single domain antibodies derived from dromedary lymph node and peripheral blood lymphocytes sensing conformational variants of prostate-specific antigen. *J. Biol. Chem.* **2004**, *279*, 51965−51972.
(28) Gemmete, J. J.; Mukherji, S. K. Panitumumab (vectibix). *Am. J. Neuroradiol.* **2011**, *32*, 1002−1003.
(29) Islam, J.; Riley, B. T.; Fercher, C.; Jones, M. L.; Buckle, A. M.; Howard, C. B.; Cox, R. P.; Bell, T. D. M.; Mahler, S.; Corrie, S. R. Wavelength-Dependent Fluorescent Immunosensors via Incorporation of Polarity Indicators near the Binding Interface of Antibody Fragments. *Anal. Chem.* **2019**, *91*, 7631−7638.
(30) Jeong, H. J.; Dong, J.; Ueda, H. Single-Step Detection of the Influenza Virus Hemagglutinin Using Bacterially-Produced Quenchbodies. *Sensors* **2019**, *19*, 52.
(31) Abe, R.; Ohashi, H.; Iijima, I.; Ihara, M.; Takagi, H.; Hohsaka, T.; Ueda, H. "Quenchbodies": quench-based antibody probes that show antigen-dependent fluorescence. *J. Am. Chem. Soc.* **2011**, *133*, 17386−17394.
(32) Jeong, H.-J.; Kawamura, T.; Dong, J.; Ueda, H. Q-Bodies from Recombinant Single-Chain Fv Fragment with Better Yield and Expanded Palette of Fluorophores. *ACS Sens* **2016**, *1*, 88−94.
(33) Sickmier, E. A.; Kurzeja, R. J.; Michelsen, K.; Vazir, M.; Yang, E.; Tasker, A. S. The Panitumumab EGFR Complex Reveals a Binding Mechanism That Overcomes Cetuximab Induced Resistance. *PLoS One* **2016**, *11*, No. e0163366.
(34) Kabat, E. A.; Te Wu, T.; Perry, H. M.; Foeller, C.; Gottesman, K. S. *Sequences of proteins of immunological interest.* (DIANE publishing) (1992).
(35) Lunder, M.; Bratkovič, T.; Kreft, S.; Štrukelj, B. Peptide inhibitor of pancreatic lipase selected by phage display using different elution strategies. *J. Lipid Res.* **2005**, *46*, 1512−1516.
(36) Chatterjee, A.; Guo, J.; Lee, H. S.; Schultz, P. G. A genetically encoded fluorescent probe in mammalian cells. *J. Am. Chem. Soc.* **2013**, *135*, 12540−12543.
(37) Lou, J.; Marks, J. D. in *Antibody Engineering.* (eds Kontermann, R.; Dübel, S.) 377−396 (Springer Berlin Heidelberg, 2010). DOI: 10.1007/978-3-642-01144-3_25
(38) Weitzner, B. D.; Jeliazkov, J. R.; Lyskov, S.; Marze, N.; Kuroda, D.; Frick, R.; Adolf-Bryfogle, J.; Biswas, N.; Dunbrack, R. L.; Gray, J. J. Modeling and docking of antibody structures with Rosetta. *Nat. Protoc.* **2017**, *12*, 401−416.
(39) Chothia, C.; Lesk, A. M. Canonical structures for the hypervariable regions of immunoglobulins. *J. Mol. Biol.* **1987**, *196*, 901−917.
(40) Marks, C.; Deane, C. M. Antibody H3 Structure Prediction. *Comput. Struct. Biotechnol. J.* **2017**, *15*, 222−231.
(41) Delgado, J.; Radusky, L. G.; Cianferoni, D.; Serrano, L. FoldX 5.0: working with RNA, small molecules and a new graphical interface. *Bioinformatics* **2019**, *35*, 4168−4169.
(42) Weber, D. S.; Warren, J. J. The interaction between methionine and two aromatic amino acids is an abundant and multifunctional motif in proteins. *Arch. Biochem. Biophys.* **2019**, *672*, No. 108053.
(43) Panousis, C.; Dhagat, U.; Edwards, K. M.; Rayzman, V.; Hardy, M. P.; Braley, H.; Gauvreau, G. M.; Hercus, T. R.; Smith, S.; Sehmi, R.; et al. CSL311, a novel, potent, therapeutic monoclonal antibody for the treatment of diseases mediated by the common β chain of the IL-3, GM-CSF and IL-5 receptors. *mAbs* **2016**, *8*, 436−453.
(44) Rich, R. L.; Papalia, G. A.; Flynn, P. J.; Furneisen, J.; Quinn, J.; Klein, J. S.; Katsamba, P. S.; Waddell, M. B.; Scott, M.; Thompson, J.; et al. A global benchmark study using affinity-based biosensors. *Anal. Biochem.* **2009**, *386*, 194−216.
(45) Vendel, M. C.; Favis, M.; Snyder, W. B.; Huang, F.; Capili, A. D.; Dong, J.; Glaser, S. M.; Miller, B. R.; Demarest, S. J. Secretion from bacterial versus mammalian cells yields a recombinant scFv with

variable folding properties. *Arch. Biochem. Biophys.* **2012**, *526*, 188−193.
(46) Lemeulle, C.; Chardès, T.; Montavon, C.; Chaabihi, H.; Mani, J.-C.; Pugnière, M.; Cerutti, M.; Devauchelle, G.; Pau, B.; Biard-Piechaczyk, M. Anti-digoxin scFv fragments expressed in bacteria and in insect cells have different antigen binding properties. *FEBS Lett.* **1998**, *423*, 159−166.
(47) Yusakul, G.; Sakamoto, S.; Nuntawong, P.; Tanaka, H.; Morimoto, S. Different expression systems resulted in varied binding properties of anti-paclitaxel single-chain variable fragment antibody clone 1C2. *J. Nat. Med.* **2018**, *72*, 310−316.
(48) Yang, D.; Singh, A.; Wu, H.; Kroe-Barrett, R. Comparison of biosensor platforms in the evaluation of high affinity antibody-antigen binding kinetics. *Anal. Biochem.* **2016**, *508*, 78−96.
(49) Schoukroun-Barnes, L. R.; Macazo, F. C.; Gutierrez, B.; Lottermoser, J.; Liu, J.; White, R. J. Reagentless, Structure-Switching, Electrochemical Aptamer-Based Sensors. *Annu. Rev. Anal. Chem.* **2016**, *9*, 163−181.
(50) Idili, A.; Parolo, C.; Ortega, G.; Plaxco, K. W. Calibration-Free Measurement of Phenylalanine Levels in the Blood Using an Electrochemical Aptamer-Based Sensor Suitable for Point-of-Care Applications. *ACS Sens* **2019**, *4*, 3227−3233.
(51) Idili, A.; Arroyo-Currás, N.; Ploense, K. L.; Csordas, A. T.; Kuwahara, M.; Kippin, T. E.; Plaxco, K. W. Seconds-resolved pharmacokinetic measurements of the chemotherapeutic irinotecan in situ in the living body. *Chem. Sci.* **2019**, *10*, 8164−8170.
(52) Li, H.; Somerson, J.; Xia, F.; Plaxco, K. W. Electrochemical DNA-Based Sensors for Molecular Quality Control: Continuous, Real-Time Melamine Detection in Flowing Whole Milk. *Anal. Chem.* **2018**, *90*, 10641−10645.
(53) Idili, A.; Gerson, J.; Parolo, C.; Kippin, T.; Plaxco, K. W. An electrochemical aptamer-based sensor for the rapid and convenient measurement of l-tryptophan. *Anal. Bioanal. Chem.* **2019**, *411*, 4629−4635.
(54) Komarova, N.; Kuznetsov, A. Inside the Black Box: What Makes SELEX Better? *Molecules* **2019**, *24*, 3598.
(55) Fontaine, F. R.; Goodall, S.; Prokop, J. W.; Howard, C. B.; Moustaqil, M.; Kumble, S.; Rasicci, D. T.; Osborne, G. W.; Gambin, Y.; Sierecki, E.; et al. Functional domain analysis of SOX18 transcription factor using a single-chain variable fragment-based approach. *mAbs* **2018**, *10*, 596−606.

https://dx.doi.org/10.1021/acssensors.0c01510
ACS Sens. 2021, 6, 764−776